

Microsegregation during Solidification of Graphitic Fiber-Reinforced Aluminum Alloys under External Heat Sinks

H.G. SEONG, H.F. LOPEZ, and P.K. ROHATGI

Squeeze casting and melt infiltration were employed in processing continuous graphitic fiber-reinforced aluminum matrix composites. The fiber reinforcements were (1) uncoated carbon fiber (UNC-CF), (2) Ni-coated carbon fiber (NiC-CF), and (3) bare graphite fibers (GRFs), and they were externally cooled to enhance the local solidification of the matrix alloy. The solidified microstructures and their composition profiles were examined using optical microscopy, scanning electron microscopy–energy-dispersive X-ray, and electron probe microanalysis–wavelength-dispersive X-ray. The resultant microstructures in the UNC-CF and NiC-CF–reinforced composites exhibited significant differences from those found in the GRF-reinforced composite, in terms of solidified morphologies and compositions. It was found that coarse columnar dendrites developed in the fiber-free matrix, fine equiaxed dendrites in the chilled matrix, and columnar-like arms in the fiber-reinforced matrices. In contrast, in bare GRF-reinforced composites, two distinct regions were clearly distinguished: (1) a region consisting of coarse equiaxed dendrites in the fiber-free matrix and (2) a featureless morphology within the fiber reinforcement regions. These distinct microstructures were attributed to preferential heat extraction through the GRFs, which possess a relatively high thermal conductivity. Apparently, heat extraction through the GRFs led to the formation of single α -Al envelopes on the fiber surfaces. In addition, the extent of solute segregation found in the GRF-reinforced alloy composite was relatively small when compared with the CF-reinforced alloy composites.

DOI: 10.1007/s11661-006-9030-4

© The Minerals, Metals & Materials Society and ASM International 2007

I. INTRODUCTION

SOLUTE distribution at the microscale level, also known as microsegregation, is an important phenomenon, which occurs during the evolution of the solidification structure. Microsegregation can lead to nonhomogeneous properties, particularly when secondary processing is not involved. Hence, extensive efforts have been made aimed at measuring and predicting solute microsegregation effects in Al alloys during solidification. Martorano *et al.*^[1] found that the extent of solute segregation in aluminum alloys is strongly influenced by the cooling rates, with severe microsegregation effects expected at reduced cooling rates. Moreover, the role of solute segregation on the secondary precipitation reactions has been investigated in some detail by several authors.^[2–4] In particular, it has been found that as the extent of microsegregation increases, secondary precipitation is effectively promoted. Nevertheless, the effect of processing parameters on the extent of microsegregation during the solidification of fiber-reinforced Al-composites has not been investigated in detail.

From the available literature on fiber-reinforced Al alloys,^[5–7] it is apparent that the extent of solute

segregation is strongly influenced by the type, volume fraction, and morphology of fibers, as well as by the melt cooling rates and alloy chemistry. Gungor *et al.*^[5] found that in an $\text{Al}_2\text{O}_3(\text{F})$ -reinforced Al-Cu alloy, a dendritic structure with normal solute coring develops within the fiber interstices when the interfiber spacing, λ_F , exceeds the secondary dendrite arm spacing, λ_{DAS} . In particular, the exhibited minimum Cu contents were found to increase linearly with $1/\lambda_F$.^[6] Moreover, the minimum Cu segregation levels in the local matrix surrounding the fibers tended to increase as the mean λ_F was reduced, or the solidification times were increased. Mortensen *et al.*^[7] investigated the microsegregation effects in directionally solidified Al-4.5 wt pct Cu alloys reinforced with $\text{Al}_2\text{O}_3(\text{F})$. In their work, the minimum Cu contents were found to increase with increasing local solidification times (above 750 seconds). These times were significantly large when compared with those found in unreinforced Al-4.5 wt pct Cu alloys under similar cooling conditions. In addition, no eutectic phases were detected on the alumina fiber interfaces, nor in the local matrix surrounding the fibers. In contrast, when the reinforced alloy was solidified within 1 second, a eutectic constituent was found to form in the reinforced matrix, preferentially along the dendrite boundaries. In other related works, Petitcorps *et al.*^[8] found that in short Al_2O_3 fiber-reinforced Al-7Si-0.3Mg and Al-7Si-2.2Mg composites, the level of Mg segregation in high Mg composites was roughly 5 wt pct higher at the fiber/

H.G. SEONG, H.F. LOPEZ, and P.K. ROHATGI are with the Department of Materials Engineering, University of Wisconsin–Milwaukee, Milwaukee, WI 53211, USA. Contact e-mail: hlopez@uwm.edu
Manuscript Submitted May 20, 2005.

matrix interfaces than that in the bulk. Similarly, for low Mg composites, the Mg content was 0.5 wt pct higher at the fiber/matrix interfaces in the reinforced matrix than in the unreinforced matrix. In this case, the segregation profiles did not exhibit any significant differences after age hardening (particularly in low Mg composites). Consequently, the composites did not respond well to T6 aging treatments, where fine Mg_2Si phases were found to form within the matrix, but relatively coarse ones were found at the fiber/matrix interfaces.

Most of the published literature has been focused on the solidification kinetics and solute segregation within fiber-reinforced regions in $Al_2O_3(F)$ -reinforced Al. However, there are no reports on the thermal effects associated with external cooling of the reinforcing fibers. Moreover, there is very limited information on the microsegregation effects in squeeze-cast fiber-reinforced composites. Yet, it is expected that microsegregation and solidification events at matrix/fiber interfaces will be strongly modified as the heat of solidification is effectively extracted through the fiber reinforcements. Hence, the present work investigates the role of external fiber cooling on the solidification morphologies and resultant microsegregation in fiber-reinforced 2014 aluminum composites.

II. EXPERIMENTAL

A series of AA2014 alloy composites reinforced with three different types of graphitic fibers were produced using a modified squeeze infiltration casting. In this setup, the fiber ends were extended outside the mold and were cooled in either air at 25 °C or in a dry ice-acetone mixture (−78 °C) (Figure 1). The fibers employed in this study were uncoated carbon fibers (UNC-CFs), Ni-coated carbon fibers (NiC-CFs), and bare graphite fibers (GRFs). The compositions of the AA 2014 alloy including some of the relevant fiber properties are given in Table I. Tows of graphitic fibers of 40 cm in length, which consisted of about 5000 filaments per bundle relative to CFs, were placed longitudinally along the parting line of a BN-coated rectangular mild steel mold. The mold design includes an extension from both mold ends to enable the housing of fibers for direct heat extraction from the solidifying melt. The wall mold thickness was 2 cm on all sides.

All of the composites investigated in this study were produced under identical processing conditions: a melt temperature of 800 °C, a mold preheating temperature of 500 °C, and an applied pressure of 32 MPa. The AA2014 alloy (500 g) was melted in a BN-coated clay graphite crucible placed in an induction furnace. The steel mold including the graphitic fiber bundle was heated to 500 °C in a heat resistance furnace filled with nitrogen gas to remove any moisture adsorbed on the fiber surfaces and to promote complete melt infiltration. The K-type thermocouples with 1-mm tip sizes were used for melt temperature measurements at selected locations of the fiber reinforcements (Figure 1). Average cooling rates and local solidification times were estimated from time-temperature curves, using a Fluke data logger connected to a data acquisition system.

Various composite samples, 8 cm × 2 cm × 7 cm, were produced using squeeze infiltration and casting. After complete infiltration and casting, the solidified composites were sectioned in the directions parallel and normal to the fiber alignment. These specimens were then polished and etched using Keller's reagent to reveal the solidification structure of the alloy matrix. The microstructural features were examined using a scanning electron microscope (SEM) and an optical microscope equipped with a digital image analyzer. In addition, electron probe microanalysis was conducted at various locations across the longitudinal sections of the fiber-reinforced 2014 alloy composites. For this purpose, a CAMECA SX-50 scanning electron microprobe equipped with a wavelength-dispersive spectrometer was employed. Only the distributions of substitutional elements were examined in these measurements using five pure elements and MgO as standards. Determinations of minimum solute concentrations were made by line scans of data points measured at 1- μ m intervals across aligned fibers in unetched longitudinal specimen sections. Then, the first lowest compositional values were selected from all the measurements and averaged with the second or third lowest ones for increasing accuracy. These measurements excluded any compositions associated with eutectic phases precipitated at either local interdendritic areas or at the fiber/matrix interfaces.

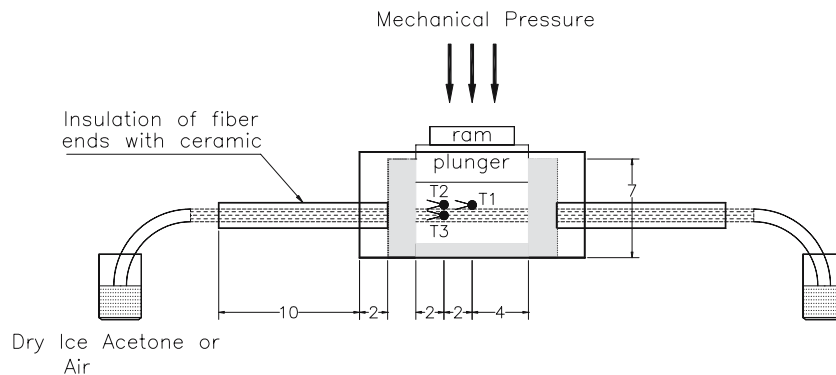


Fig. 1—Schematic diagram showing the mold dimensions (cm) and thermocouple locations (T). T1 and T2 are located on fiber surface tows at 4 and 2 cm from one edge of the mold, while T3 is inside the reinforced fibers at a similar location as T2.

Table I. Nominal Composition of Alloy and Selected Properties of Used Continuous Fiber

Materials	Composition					
	Cu (Wt Pct)	Si (Wt Pct)	Mg (Wt Pct)	Mn (Wt Pct)	Fe (Wt Pct)	Al (Wt Pct)
AA2014	4.5	0.7 to 0.9	0.5	0.8	0.25	bal
Continuous Fiber	Tensile Strength (MPa)	Tensile Modulus (GPa)	Axial TC (W/m °C)	Diameter (μm)	Density (g/cm ³)	Carbon (At. Pct)
Uncoated PAN CF	3450	217	20	6 to 8	1.8	95
Ni coated PAN CF	2820	212	90.9 ⁺ (pure Ni)	6 to 8	2.206	20 to 26 (Ni)
Uncoated pitch graphite fiber	3100	931	1000	10	2.2	99

III. RESULTS

A. Microstructures of As-Cast Composites

Table II shows the estimated cooling rates and solidification times obtained from the cooling curves for the various composites. Also, Figure 2 shows the transverse microstructures for the Al alloy composites reinforced with three different continuous fibers externally cooled in a dry ice-acetone mixture. The solidification microstructures consisted of primary α -Al, as well as secondary phases at the interdendritic boundaries or in the vicinity of the reinforced fibers. In both UNC-CF- and NiC-CF-reinforced composites (Figures 2(a) through (c) and 2(d) through (f)), coarse columnar dendrites with long trunks were found to be fully developed in the unreinforced alloy matrix regions (region A) far from the reinforced fibers. In contrast, fine equiaxed dendrites were found in the matrix region surrounding the periphery of the reinforced regions (region B). Apparently, the refined microstructures found in region B were promoted by relatively high cooling rates as a result of external cooling from the fiber ends in a dry-ice/acetone. Measured local solidification times, t_f , of 62 and 103 seconds were experimentally found for UNC-CF- and NiC-CF-reinforced composites, respectively. In contrast, in air-cooled bare GRF-reinforced composite, the t_f value was 117 seconds at a range between start of solidification and 500 °C, as shown in Table II. In addition, the equiaxed dendrites developed in

the surroundings of the reinforcing GRF composites were relatively coarse, suggesting the lack of a significant increase in cooling rates due to the presence of fibers in this region. In the reinforced matrix (region C) of UNC-CF and NiC-CF composites, appreciable refinement of the α -Al arms was found to occur (Figures 2(c) and (f)) within narrow fiber interstices, with coarsening being increasingly dominant at relatively large λ_F . In particular, at large λ_F eutectic precipitation, ($\alpha + \theta$ -CuAl₂) was found to occur to some extent, connecting neighboring fibers, as well as quaternary phases. Moreover, the reinforcing fibers were not very uniformly distributed. In contrast, in the GRF-reinforced composites, a dendritic structure did not seem to develop within the interfiber regions (Figure 2(i)). Also, there was hardly any precipitation of secondary phases between fibers or at fiber/matrix interfaces.

Figure 3 shows the longitudinal microstructures exhibited in squeeze-cast 2014 alloy composites. From these figures, it is evident that there are no significant differences in the solidification microstructures produced by the various heat sinks employed (Figures 3(a) through (f)). Nevertheless, the measured size differences for similar λ_F were roughly 10 μm ($\lambda_{DAS} = 24$ to 26 μm and 35 to 36 μm for UNC-CF and NiC-CF cooled in dry ice-acetone, respectively, and 35 to 40 μm in air-cooled GRF). The final morphologies of fully grown arms were quite similar for both UNC-CF and NiC-CF

Table II. Measured Thermal Parameters in Externally Cooled Composites at T2 and T3*

Material	Parameters			
	Cooling Rate CR (°C/s)		Local Solidification Time t_f (s), up to 550 °C	
	Reinforced (T3)	Chilled (T2)	Reinforced (T3)	Chilled (T2)
AA2014 only		4		—
Air-cooled (I) CF 2014	10	13	62	19
Dry-ice acetone cooled (II) UNC CF 2014	—	18	32	11
Air-cooled (I) NiC CF 2014	5	10	103	68
Dry ice-acetone cooled (II) NiC CF 2014	8	—	80	—
Air-cooled (I) GrF 2014	4	6	16 (641 °C to 580 °C) 117 (641 °C to 500 °C)	16 (641 °C to 580 °C) 117 (641 °C to 500 °C)
Dry ice-acetone cooled (II) UNC GrF 2014	—	—	—	—

*Forty-nine seconds is the solidification time corresponding to cooling to 550 °C.

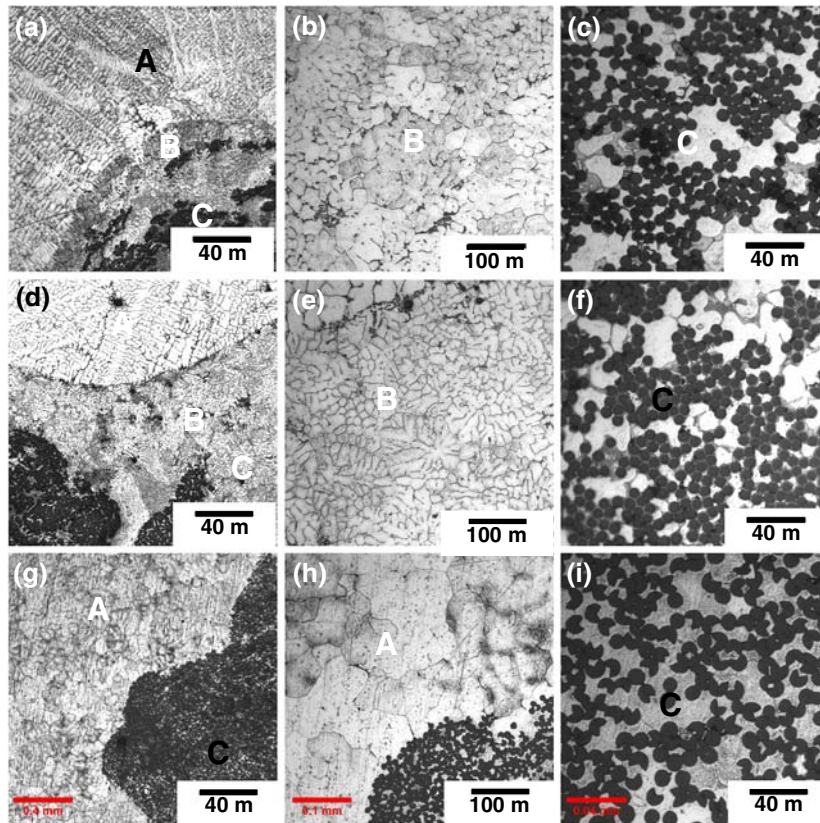


Fig. 2—Transverse microstructures of squeeze-cast 2014 alloy composites reinforced with externally cooled fibers in a dry ice-acetone mixture at three regions: A = unreinforced matrix, B = chilled matrix, and C = reinforced matrix. (a) through (c) UNC-CF composites, (d) through (f) NiC-CF composite, and (g) through (i) GRF composite.

composites. In these composites, dendritic arms with side branches were found at large λ_F (above $30 \mu\text{m}$), but they became rather featureless at small λ_F (below $30 \mu\text{m}$). On the other hand, in GRF composites, the fully grown primary $\alpha\text{-Al}$ was coarse and featureless regardless of the actual λ_F values. This, in turn, suggested that during solidification, the solid/liquid interface was essentially planar. Only a negligible volume fraction of secondary phases was found to precipitate at interarm locations or to connect other fiber/matrix interfaces.

Figure 4 is an SEM photograph of secondary phases as well as their compositions found in an air-cooled UNC-CF composite. Notice the presence of a relatively large blocky phase ($\text{Al}_{15}(\text{CuFeMn})_3\text{Si}_2$, marked as I), connected to the eutectic constituent (marked as II) in the interdendritic regions. In addition, a black phase identified as Mg_2Si was found to form next to eutectic lamellae (marked as III). The morphology of the precipitated phases suggests that solute is laterally rejected as primary $\alpha\text{-Al}$ grows longitudinally within the fiber interstices. In particular, notice that secondary phase precipitation at fiber interfaces is not favored, as evidenced by the rather low precipitation frequency at these locations. X-ray diffraction peaks corresponding to secondary phases found in the base alloy and in the fiber-reinforced composites are shown in Figure 5.

From this figure, the only secondary phases positively identified by XRD were $\theta\text{-CuAl}_2$ and Al_2CuMg .

B. Solute Segregations of As-Cast Composites

Solute concentration profiles were measured at various cross sections normal to the longitudinal fiber directions for each of the composites investigated in this work. Figure 6 shows the exhibited concentration profiles for various alloying elements (Fe, Mn, Cu, Mg, and Si) measured across solidified arms between the reinforcements. Notice from Figures 6(a) and (b) that with the exception of Mn, the lowest solute compositions were found at the center of the solidified arms. Moreover, the largest solute enrichment was present at the fiber/matrix interfaces in both air-cooled UNC-CF- and NiC-CF-reinforced composites. However, in the GRF composites, the solute distribution profiles indicated that there were hardly any fluctuations in solute composition within the matrix across fiber regions. This, in turn, indicated that the matrix solute composition was highly homogeneous. In particular, Mn and Fe seemed to be evenly distributed, even though their actual contents were relatively low when compared with the other elements.

Figures 7(a) through (f) are plots of minimum solute content as a function of λ_F exhibited in the three

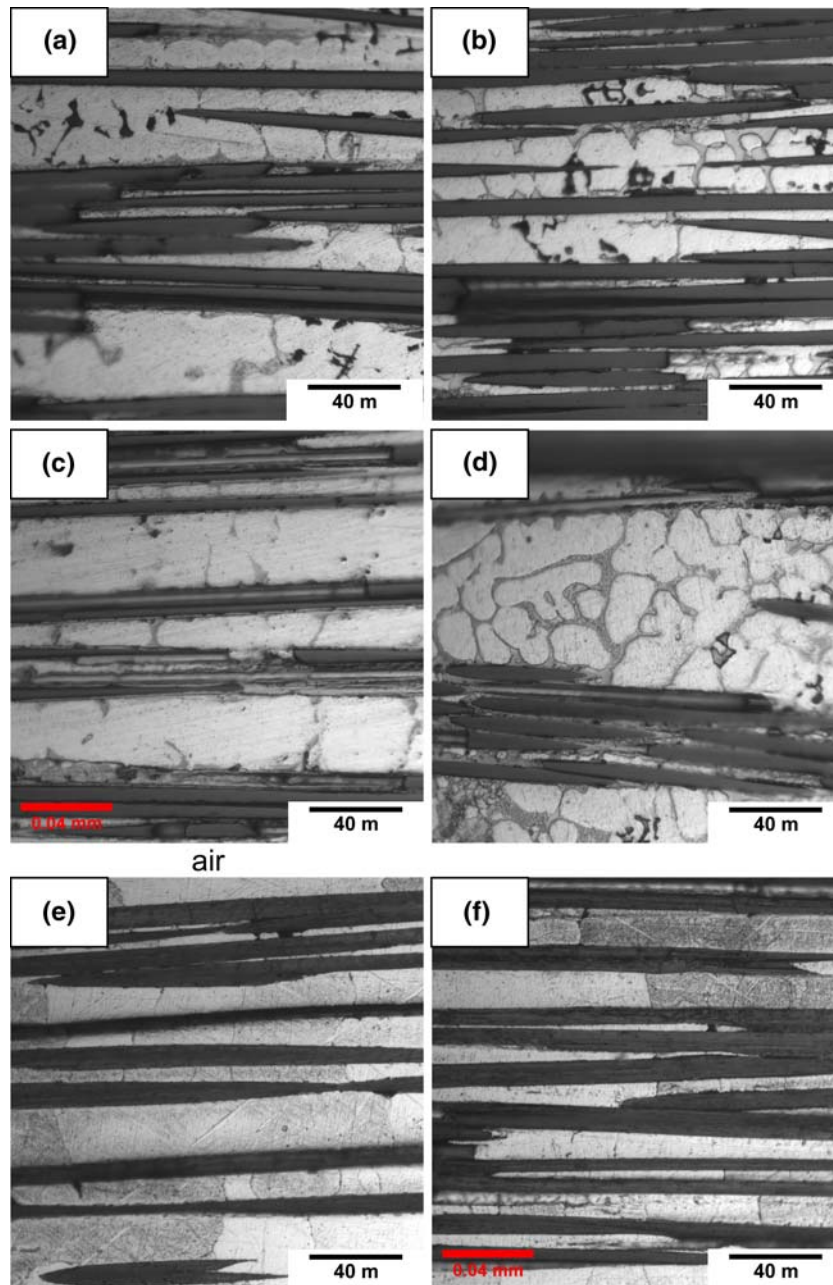


Fig. 3—Longitudinal microstructures of squeeze-cast AA 2014 alloy composites reinforced with externally cooled fibers (*a*), (*c*), and (*e*) in air and (*b*), (*d*), and (*f*) in dry ice-acetone. (*a*) and (*b*) UNC-CF composite, (*c*) and (*d*) NiC-CF composite, and (*e*) and (*f*) GRF composite.

air-cooled alloy composites. Notice that in the case of Cu, the minimum contents tend to increase linearly with $1/\lambda_F$. The minimum Cu contents found in the GRF composite are somewhat above those corresponding to UNC-CF and NiC-CF composites (Figures 7(e) and (f)).

The variation in minimum solute contents with distance from the mold walls was also determined in this work, and the results are given in Table III. The compositional measurements were made at similar λ_F , but at distance intervals of 1 and 2 cm. It was found that the minimum solute contents for an equivalent λ_F were slightly low in the reinforced matrix near the edge of the

mold (at 1 cm), but they increased toward the center of the reinforced matrix (2 cm from the edge of the mold). This, in turn, indicated that the minimum solute contents tend to decrease with increasing cooling rates, as expected for external fiber cooling conditions. In other words, the relatively slow solidification rates expected as one moves away from the mold edge promote enough solute diffusivity to enhance the minimum solute contents. This trend was not clear in NiC-CF composites, where some of the Ni layer might get dissolved in the melt (Figure 7). Thus, it is apparent that Ni dissolution modifies the resultant solute distribution profiles, as well as the matrix chemistry.

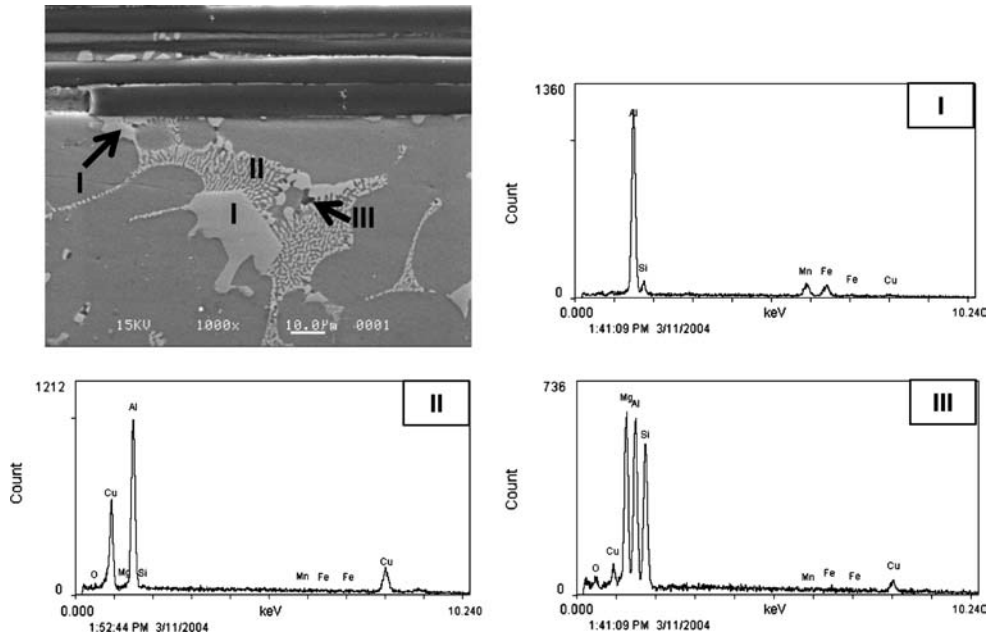


Fig. 4—SEM micrograph and EDS spectra (I, II, and III) showing the chemistry of precipitated phases in the reinforced matrix in an air-cooled CF composite. I = blocky phase (dark gray) = $\text{Al}_{15}(\text{CuFeMn})_3\text{Si}_2$, WDX analysis, 77.21 Al at. pct, 6.70 Si at. pct, 6.61 Cu at. pct, 5.53 Mn at. pct, and 3.38 Fe at. pct; II = eutectic phase = CuAl_2 ; and III = black phase = Mg_2Si .

IV. DISCUSSION

A. Microstructure

The experimental outcome of the present work clearly shows a transition in the dendritic structure of primary α -Al as heat is extracted through the fiber reinforcements (Figures 2 and 3). In UNC-CF and NiC-CF composites, the morphological changes exhibited in the solidified structures can be described as going from columnar dendrites in the unreinforced matrices to refined equiaxed dendrites in the neighborhood of the reinforcements, and to dendritic and cellular structures within the reinforced matrix regions. The development of fine equiaxed dendrites in the locally chilled matrices can be attributed to a local increase in the extent of melt undercooling, ΔT , as a result of heat dissipation through the fiber ends and solute buildup within the melt. Accordingly, appreciable nucleation events were highly favored in the undercooled melt surrounding the carbon fibers leading to the development of fine equiaxed dendrites in the chilled matrix regions. It is well known^[10] that the nucleation density, N , is directly related to the degree of undercooling and to the physical-chemical state of the melt through $N = K\Delta T^n$, where K and n are experimentally determined constants. Thus, as ΔT increases, so does the potential density of nuclei formed in the undercooled melt accounting for the exhibited refinement in the dendritic matrix microstructure.

Alternatively, the solidified microstructures found in the CF-reinforced composite regions were not present in the GRF composites. Instead, coarse dendrites were found in the matrix regions near, but away from, the GRF reinforcements and a solidified featureless

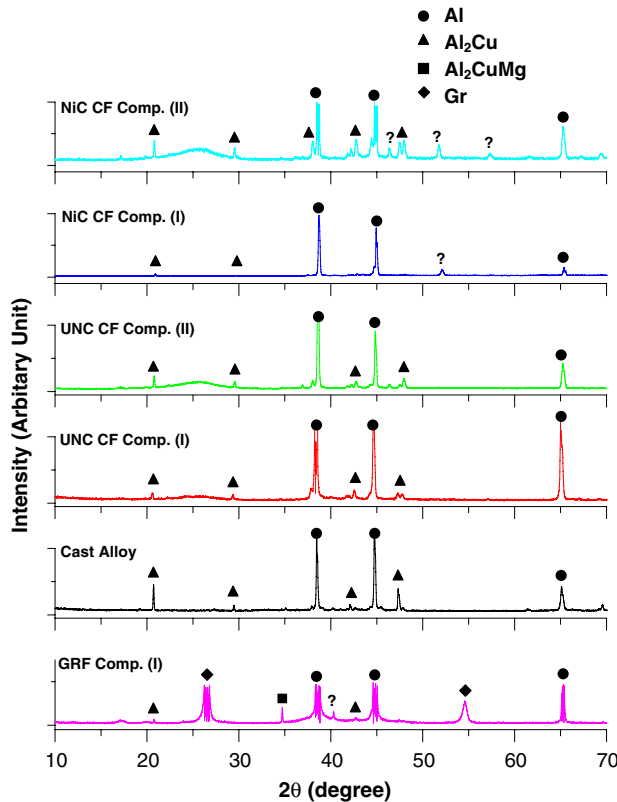


Fig. 5—X-ray diffraction peaks for the squeeze-cast 2014 alloy composites. Notice that only CuAl_2 and CuAl_2Mg precipitates are positively identified.

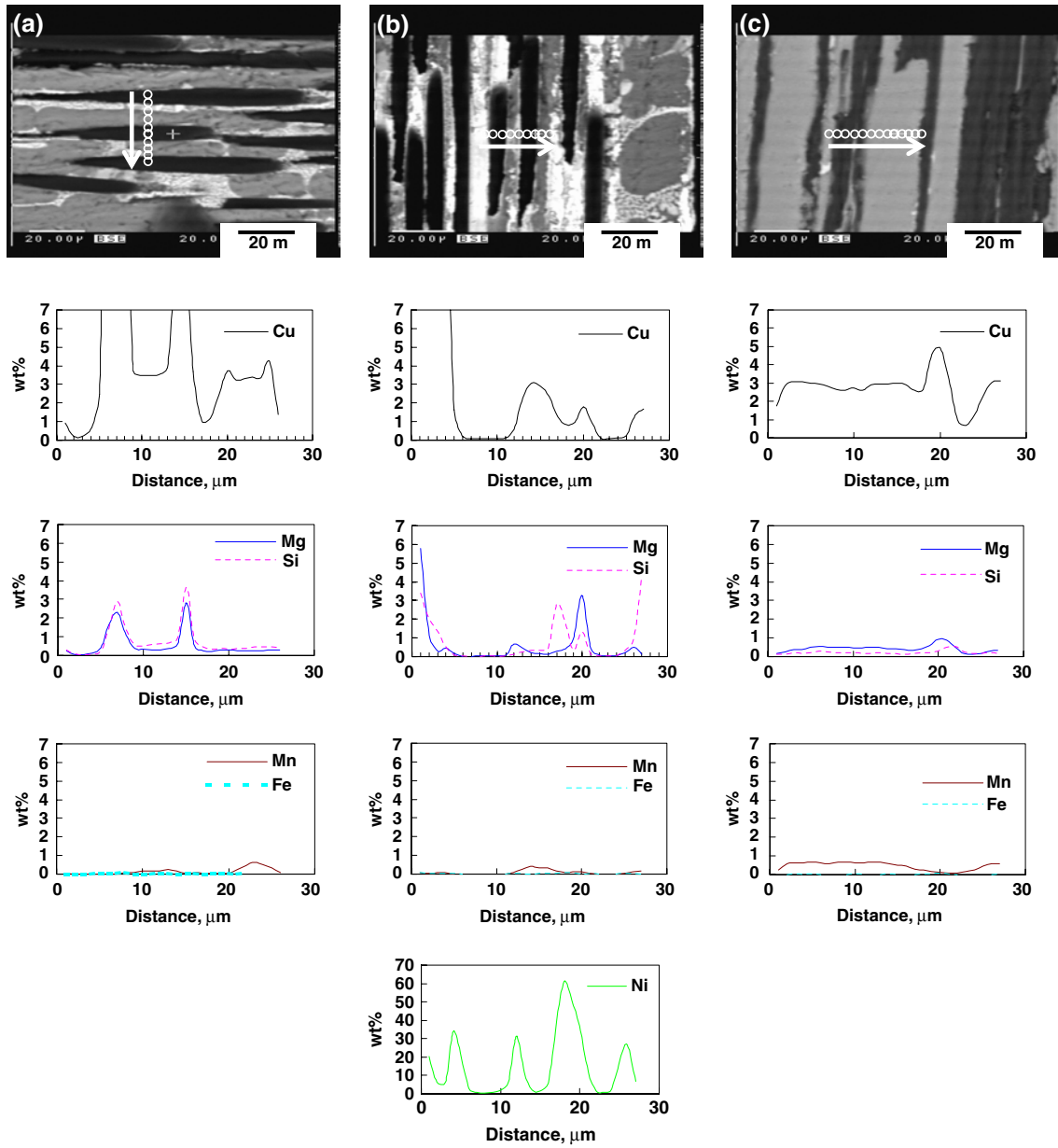


Fig. 6—Solute concentration profiles found in the solidified matrix surrounding the air-cooled fiber reinforcements for three 2014 composites: (a) uncoated CF composite, (b) Ni-coated CF composite, and (c) GRF composite.

structure within the fiber interstices. This, in turn, indicated that the externally cooled GRFs act as effective chills for rapid heat extraction from the melt. Flemings and co-workers^[9] have considered the effect of a chill on the overall local undercooling at a dendrite tip in solidification of a Fe-Cr-Ni alloy. In their proposed model, a positive temperature gradient is assumed to develop at the solid/chill (thermal undercooling), while a negative gradient is present at the dendrite tip due to solutal, curvature, and kinetic undercoolings associated with the undercooled melt. The model predictions clearly show that high heat extraction rates through the chill substrate promote planar growth. Moreover, under these conditions, increasing melt undercoolings are needed to maintain dendritic growth. The

solidification conditions investigated by Flemings and co-workers^[9] are somewhat similar to the ones developed in the GRF composite system, implying that there is a lack of significant undercooling in the surrounding melt. Figure 8 (a) shows the cooling curves exhibited by the three fiber-reinforced composites. Notice that the local melt temperature ($T_{L(max)}$) in the GRF-reinforced composite was the lowest when compared with the ones corresponding to UNC-CF and NiC-CF composites. In addition, the estimated local melt undercoolings, $\Delta T_L = (T_{L(max)} - T_{L(min)})$ were in decreasing order, 0.3 °C in uncoated CFs, 0.1 °C in Ni-coated CFs, and nonmeasurable for the GRFs when the fiber ends were air-cooled. The actual extent of undercooling might be somewhat higher than what was actually measured due

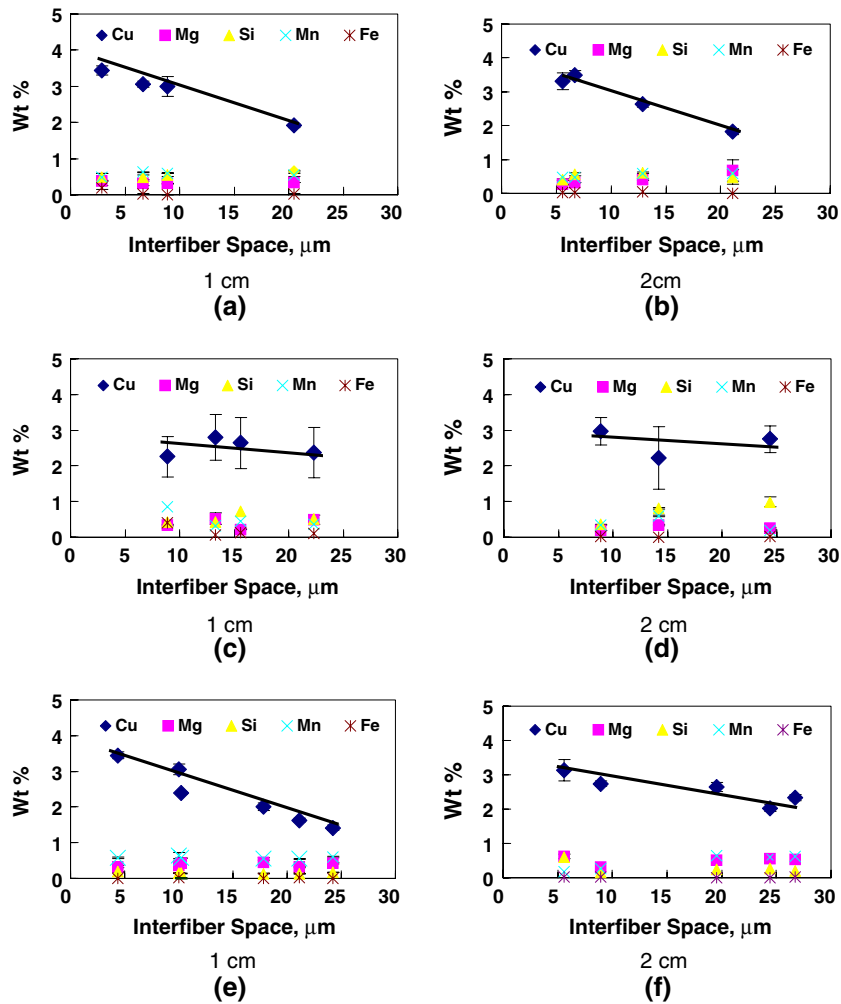


Fig. 7—Minimum solute contents as a function of interfiber spacing at two locations for air-cooled fiber-reinforced composites: (a) and (b) uncoated CF composite, (c) and (d) Ni-coated CF composite, and (d) and (e) GRF composite.

Table III. Minimum Solute Contents in Alloy Matrices as a Function of Distance from the Mold Wall (Weight Percent)

Element	Composite					
	UNC CF 2014		NiC CF 2014		GRF 2014	
	IFS* = 6.67 μm		IFS = 8.9 μm		IFS = 24.4 μm	
	1 cm	2 cm	1 cm	2 cm	1 cm	2 cm
Cu	1.61	1.88	0.98	1.15	0.72	1.04
Mg	0.45	0.50	0.51	0.18	0.58	0.75
Si	0.58	0.74	0.28	0.49	0.20	0.30
Mn	0.39	0.09	0.14	0.18	0.33	0.37
Fe	0.02	0.03	0.02	0.02	0.01	0.00
Al	bal	bal	bal	bal	bal	bal

*IFS = interfiber spacing.

to experimental limitations. However, these results clearly show that in the GRF-reinforced regions, significant heat extraction rates are attained during the early stages of solidification. In particular, there is no significant recalescence, which can be linked to the formation of new nuclei within the melt surrounding the chilled fibers.

At increasing melt undercoolings, cellular or dendritelike structures are strongly favored and can account for the solidification morphologies exhibited in the UNC-CF and NiC-CF composites (Figures 2 and 3). Nevertheless, in the GRF composite, the solidified morphology was essentially featureless, strongly suggesting that under external cooling exerted by GRFs, a

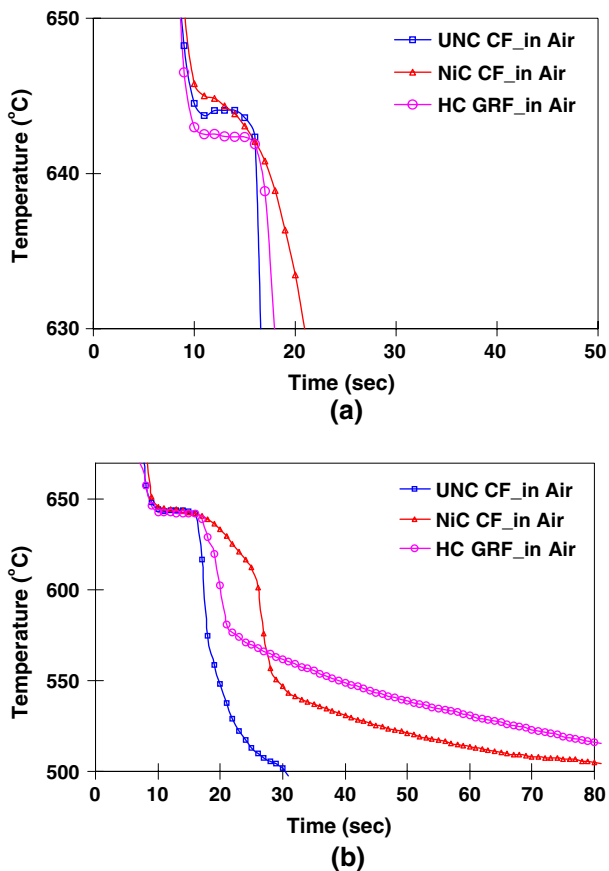


Fig. 8—(a) Cooling curves exhibited by the three squeeze-cast 2014 alloy composites externally cooled in air and measured at a fixed location (T2). (b) Enlarged view of (a) at 650 °C to 500 °C.

planar front was developed at the fiber/melt interface. In the work of Flemings and co-workers,^[9] it is found that in the presence of the chill, a planar solidification front can be stable at relatively small melt undercoolings. These conditions have been described by the proposed stability criterion:^[9]

$$-(k_L G_L \xi_L + k_S G_S \xi_S) + m_L G_C \xi_C \leq 0 \quad [1]$$

where k_L is the thermal liquid conductivity; k_S is the solid thermal conductivity; m_L is the slope of the liquidus line; ξ_S and ξ_L , are the thermal stability parameters for the solid and liquid, respectively; and ξ_C is the solutal stability parameter. From Eq. [1], a planar front can be stable when the rate of heat transfer is controlled by the thermal gradient in the solid chill ($G_S > 0$) and by the gradient caused by the liquid concentration gradient ($m G_C > 0$). Moreover, at relatively large melt undercoolings, G_C becomes negligible, and the front stability is dominated by the temperature gradient in the liquid ($G_L < 0$) and solid ($G_S > 0$).

In the present work, the apparent suppression in the exhibited $T_{L(\max)}$ values can be related to the thermal undercooling developed in the chilled GRFs as a result

of heat extraction. In principle, relatively large amounts of heat extraction are feasible in externally cooled GRFs due to their high thermal conductivities, which easily exceed the ones for the other fibers, or the liquid melt ($k_{GRF(S)} = 1000 \text{ W/m/K}$, and $k_{Al(L)} \approx 180 \text{ W/m/K} > k_{CF(S)} = 20 \text{ W/m/K}$ ^[12]). An estimation of the amount of heat extraction ($Q_{\text{ext}} = k \times \Delta T / \Delta X$) through a single reinforcing fiber, using the temperature gradient developed at two different locations ($X_2 = 2 \text{ cm}$ and $X_1 = 4 \text{ cm}$ away from the edge of the castings) as well as the surface area of the fiber, yields 0.000046 W for a CF, 0.000528 W for a Ni-coated CF, and 0.024757 W for a GRF. In these calculations, the temperature gradient was determined from the liquidus arrest temperatures exhibited in the cooling curves recorded at the two locations. Notice from these estimations that heat extraction through the GRFs is two to three orders of magnitude higher than the ones corresponding to the CF reinforcements.

Thus, in the GRF-reinforced composite, relatively high heat extraction rates through the individual cold fibers are likely to promote radial planar growth. As mentioned previously, the development of the planar front can occur at low growth velocities when the melt undercooling is relatively small and some extent of constitutional undercooling in the liquid is viable.^[11] Alternatively, planar growth can occur at high melt undercoolings, where solute trapping is prevalent and competition between the thermal gradients in the solid and liquid determine the stability of the plane front interface.^[9] Therefore, in the present work, the development of a planar interface seems to be strongly favored, as it accounts for the lack of significant melt undercooling and the relatively low growth velocities. Figure 8(b) is an enlarged view of the cooling curves exhibited by the fiber-reinforced composites showing a significant change in their slopes below 580 °C for a GRF composite. This, in turn, indicates that in the GRF composite, the growth velocity of the solidification front is relatively low when compared with the other composites investigated. Moreover, under these conditions, any solute redistribution in the liquid can account for the incipient eutectics in the solidified structures.

Other plausible explanations for the development of a planar front can be related to the role of convective melt flow. Das and Fan^[13] investigated the role of convection on the exhibited solidified morphologies in semisolid processing of a Sn-15 wt pct Pb alloy. Monte Carlo simulations indicated that turbulent flow in the direction parallel to the solidification front promotes a planar front. Yet, a dendritic structure is developed when the direction of the turbulent flow is normal to the growth direction. The stabilization of the planar front was attributed to a reduction in the thickness of the diffusion boundary layer due to turbulent flow. In this case, liquid flow penetration into the interdendritic regions was indicated to lead to the development of a flat front as solute is transported away from these regions into the bulk melt. In practice, however, the direction of convection forces is difficult to predict or to control.

Forced convective melt flow in squeeze infiltration casting might be significant, but it is unlikely that it can account for the exhibited planar growth morphologies. Depending on the direction of the convective flow, any growth morphologies can be stabilized, leading to a lack of control over the resultant microstructures. Also, the most favorable direction for convective flow within the GRF-reinforced regions should be normal to the growth direction, which is not expected to favor planar growth.^[13] Under these conditions, the convective turbulent flow might stabilize a dendritic morphology unless the initial interface remains planar. Then, convective flow is likely to promote any disturbance, tilting, from the original growth directions. Yet, no shifting in the growth directions was detected in this work, as confirmed by the exhibited XRD patterns (Figure 5).

In fiber-reinforced composite systems, the resultant growth morphologies are generally determined by the magnitudes of the dendrite arm spacings *vs* the interfiber spacings. According to other authors,^[7,14,15] a dendritic morphology typically develops when $\lambda_F > \lambda_{DAS}$, while cellular morphologies are promoted when the opposite is true. This is found to be valid when solidification takes place in the fiber interstices without external fiber cooling. As noted in the present work, however, the possible development of a solid envelope and its planar growth at individual GRFs strongly suggest that the nucleation barrier for primary α -Al on the reinforcing cold GRFs is rather small (*i.e.*, the effective wetting angle approaches zero (Figures 3(e) and (f)). In this case, any convective-melt infiltration into the fiber interstices is not expected to disrupt the solidification front, because the positive temperature gradient developed in the fiber reinforcements (*G_s*) is dominant. Moreover, the exhibited planar morphology does not seem to be influenced by any variations in the interfiber spacings. In the UNC-CF and NiC-CF composites, external fiber cooling might also promote the instantaneous development of relatively thin solidified α -Al envelopes around reinforcements as a result of external fiber cooling. As described in previous works,^[16,17] these α -Al layers apparently remelt *via* entrainment of additional molten alloy into the fiber interstices, because the heat extraction rates are not high enough to promote continuous growth of the initial α -Al layers. Under these conditions, nucleation of primary α -Al becomes preferential in the undercooled melt restrained by the surrounding fibers, resulting in either dendritic or cellular structures. In addition, during dendrite growth, side branching can occur due to local constitutional undercooling within the CF interstices. In this case, the fiber reinforcements are expected to prevent rejected solute from diffusing too far into the undercooled melt, favoring to some extent lateral diffusion-controlled growth.^[15,18] This, in agreement with the microstructures, exhibited in the CF composites where growth of α -Al cells, including side branches, was found between reinforced fibers. In particular, dendritelike morphologies were found to develop under conditions where

$\lambda_F < \lambda_{DAS}$ as a result of external fiber heat extraction (Figures 2(c) through (f) and 3(b) through (d)).

B. Microsegregation

Experimentally, relatively large differences in the solute distributions within the reinforced regions were found (Figures 6 and 7, and Table III). Comparison of the three different fiber-reinforced matrices indicates that in the GRF composite, there were hardly any fluctuations in solute composition and solute buildup. Particularly, the Cu content in the GRF composites was highly homogeneous, suggesting that the solidification front did not lead to appreciable constitutional supercooling in the undercooled melt. This further supports the experimental observations of a planar solidification front in the GRF composites. In addition, the fraction of secondary phases, including eutectics, was significantly low at the fiber/matrix interfaces and almost nonexistent in the cast GRF composites.

The minimum Cu contents measured in the GRF-reinforced matrices were also found to decrease with increasing λ_F in both cast CF and GRF composites, as similarly shown in other reported works.^[7,19,20] Liu *et al.*^[6] have also indicated that these trends are related to late solidification events when the melt is solute enriched, particularly at the narrow λ_F . However, it does not explain the experimental solute profiles found in the NiC-CF composite. Apparently, in this case, Ni dissolution apparently leads to a modification in the solute distribution profiles (Figure 7).

Among the plausible explanations for the compositional features exhibited by the GRF composites is the likelihood of Ostwald Ripening events. Mortensen and co-workers^[21] have investigated the influence of the local solidification times on the resultant microstructure, including microsegregation in fiber-reinforced matrices. In their work, it is found that increasing local solidification times and decreasing fiber interstices promote the reduction in microsegregation, as well as the eutectic fractions. The reduced microsegregation is attributed to enhanced solute backdiffusion in the solidified α -Al due to short diffusional lengths. Under these conditions, time-dependent coarsening and rapid arm coalescence are highly favored accounting for the lack of microsegregation and of any eutectic constituents. A relatively long solidification time, roughly 940 seconds, is needed for Ostwald Ripening to be effective. In the present work, however, the homogenous nature of the solute distribution in α -Al was achieved in relatively short times (≈ 100 seconds). According to the work of Li *et al.*,^[22] the total solidification of at least 520 seconds is necessary to eliminate microsegregation (with minimum Cu content of 5 wt pct) and eutectics in Al₂O₃ fiber-reinforced Al-6 wt pct Cu matrices. When $\lambda_F < \lambda_{DAS}$, the nondendritic (planar) structures also develop at total solidification time above 10 seconds. In this composite system, however, the last liquid to solidify surrounds the fiber reinforcements, resulting in the solidification of eutectic constituents predominantly at the fiber/matrix interfaces. This is in contrast with the results of the

present work, where the relatively high thermal conductivity of the graphite fibers coupled with a thermal gradient promotes the solidification of α -Al envelopes at the fiber interfaces. In the investigated composite system, any eutectic constituents develop away from the GRF/Al interface. Thus, the results of Li *et al.*^[22] cannot be used to account for the development of a planar front, nor the microsegregation profiles found in the GRF composite investigated in the present work (Figures 3(e) and (f) and 6(c)). Ostwald Ripening or backdiffusion, itself, is also unlikely to explain the reduced microsegregation in the GRF composite, as diffusional processes can be relatively sluggish. Therefore, the reduction in solute segregation shown in the GRF composite is ascribed to the development of a planar front as a result of heat extraction through the GRF reinforcements. This, in turn, might be associated with the solute partition at a relatively small deviation from the local interface equilibrium ($k = C_S^*/C_L$).

In fiber-reinforced matrices, the exhibited amounts of secondary phases formed during solidification can be related to the extent of solute segregation at the fiber/melt interfaces. Solute segregation and solute adsorption at fiber/melt interfaces can be highly favored because they provide a way for the reduction in the fiber surface energy.^[23] In the case of GRFs, the surface energy is relatively low when compared to carbon fibers due to the large number of basal planes parallel to the fiber axis. Hence, solute segregation to graphite GRF surfaces is expected to be relatively low during melt infiltration. Moreover, any segregated solutes are expected to be chemically adsorbed along short diffusion paths,^[18] presumably at intergraphite crystal boundaries, in spite of the near-zero solubility of solutes into the solid carbon or graphite.^[24] Thus, the lack of significant precipitation of eutectic constituents at the GRF interfaces can be related to small solute segregation at the fiber/melt interfaces. Wu *et al.*^[25] have examined various eutectic morphologies exhibited in CF- and GRF-reinforced Mg-based AZ81 composites. It is shown that the Mg₁₇Al₁₂ eutectic constituent is discontinuously precipitated on carbon fibers, but continuously on graphite fibers. The continuous precipitation of eutectics in their work is attributed to the lack of significant nucleation sites at the GRF/melt interfaces. Even in the GRF-reinforced 2014 aluminum composite, a similar argument can be used to account for the absence of appreciable precipitation events, as experimentally found in the present work.

V. CONCLUSIONS

The influence of direct heat extraction through external cooling of reinforcing fibers on the resultant solidified microstructures including microsegregation effects were investigated in various squeeze-cast 2014 alloy composites. The results of this work can be summarized as follows.

1. Heat extraction through the reinforcing fibers modifies the dendritic structure of primary α -Al. In CF-rein-

forced composites, chilled matrices were developed with refined equiaxed dendrite grains. Away from the fiber reinforcements, the solidified matrices consisted of long columnar dendritic grains.

2. In UNC-CF and NiC-CF composites, the solidified morphologies within the fiber interstices consisted of dendritic and cellular grains, often with arm sizes below the mean fiber spacing. However, planar growth morphology was developed in the GRF composite, regardless of the actual fiber spacings.
3. Solute segregation in the matrices surrounding the reinforcements was relatively high in UNC-CF and NiC-CF-reinforced alloy composites. In GRF-reinforced composite, yet, the solutes were homogeneously distributed. The reduction in solute segregation in the GRF composite was ascribed to the development of a planar front as a result of heat extraction through the GRF reinforcement ends.
4. In fiber-reinforced α -Al matrices, the minimum Cu solute contents increased with decreasing interfiber spacings in both UNC-CF and GRF composites, but no consistent trend was found in the NiC-CF composites. All of the other elements also appeared to decrease or remain constant with decreasing interfiber spacings.

ACKNOWLEDGMENTS

This research work was supported by the United States National Science Foundation (NSF) under Contract No. CMS 9821057.

REFERENCES

1. M.A. Martorano and J.D.T. Capocchi: *Metall. Mater. Trans. A*, 2000, vol. 31A, pp. 3137–48.
2. T.F. Bower, H.D. Brody, and M.C. Flemings: *Trans AIME*, 1966, vol. 236, pp. 624–36.
3. X.-Y. Yan, Y.A. Chang, F.-Y. Xie, S.-L. Chen, F. Zhang, and S. Daniel: *J. Alloys Compounds*, 2001, vol. 320, pp. 151–60.
4. X. Yan, S. Chen, F. Xie, and Y.A. Chang: *Acta Metall.*, 2002, vol. 50, pp. 2199–2207.
5. M.N. Gungor: *Metall. Trans. A*, 1989, vol. 20A, pp. 2529–33.
6. H.-N. Liu, K. Ogi, and H. Miyahar: *J. Mater. Sci.*, 1998, vol. 33, pp. 3615–22.
7. A. Mortensen and M.C. Flemings: *Metall. Mater. Trans. A*, 1996, vol. 27A, pp. 595–609.
8. Y. Le Petitcorps, J.M. Quenisset, G. Le Borgne, and M. Barthele: *J. Mater. Sci. Eng. A*, 1991, vol. 135(1–2), pp. 37–40.
9. T. Koseki and M.C. Flemings: *Iron Steel Inst. Jpn. Int.*, 1995, vol. 35(6), pp. 611–17.
10. E. Fras and H.F. Lopez: *Int. J. Cast Met. Res.*, 2000, vol. 12, pp. 283–92.
11. M.C. Flemings: *Solidification Processing*, McGraw-Hill, New York, NY, 1974 60.
12. T.W. Clyne *Comprehensive Composite Materials*, Pages 447–68, in *MMCs*, T.W. Clyne, ed. Vol. 3, Elsevier, New York, NY, 2000, pp. 447–68.
13. A. Das and Z. Fan: *Mater. Sci. Eng. A*, 2004, vol. A365, pp. 330–35.
14. J.A. Sekhar and R. Trivedi: *Mater. Sci. Eng.*, 1989, vol. A114, pp. 133–46.
15. R. Trivedi, S.H. Han, and J.A. Sekhar: *Conf. on Solidification of Metal Matrix Composites*, P.K. Rohatgi, ed., TMS, Warrendale, PA, 1990, pp. 23–27.

16. A. Mortensen, L.J. Masur, J.A. Cornie, and M.C. Flemings: *Metall. Trans. A*, 1989, vol. 20A, pp. 2535–47.
17. A. Mortensen and V. Michaud: *Metall. Trans. A*, 1990, vol. 21A, pp. 2059–72.
18. R. Asthana: *J. Mater. Sci.*, 1998, vol. 33, pp. 1679–98.
19. H. Miyahara and K. Ogi: *Mater. Trans.*, 2001, vol. 42(2), pp. 258–62.
20. H. Miyahara and K. Ogi: *Mater. Trans.*, 2001, vol. 42(2), pp. 252–57.
21. A. Mortensen, J.A. Cornie, and M.C. Flemings: *Metall. Trans. A*, 1988, vol. 19A, pp. 709–21.
22. Q.F. Li, D.G. McCartney, and A.M. Walker: *J. Mater. Sci.*, 1991, vol. 26, pp. 3565–74.
23. W.D. Kaplan: *Acta Mater.*, 1998, vol. 46(7), pp. 2369–79.
24. C. Qiu and R. Metselaar: *J. Alloys Compounds*, 1994, vol. 216, pp. 55–60.
25. F. Wu and J. Zhu: *Comp. Sci. Technol.*, 1997, vol. 57, pp. 661–67.